Glucose oxidation on gold in alkaline solution: A DEMS and microkinetic modeling study

Théo Faverge, Antoine Bonnefont, Marian Chatenet, Christophe Coutanceau

Glucose oxidation on gold in alkaline solution: a DEMS and microkinetic modelling study

Théo Faverge[1,2], Antoine Bonnefont[2], Marian Chatenet[2], Christophe Coutanceau[1]

[1]*IC2MP, UMR 7285 CNRS-University of Poitiers; 4 rue Michel Brunet, TSA 51106, 86073 Cedex 9 Poitiers, France*

[2]*LEPMI, UMR 5279 CNRS-University Grenoble Alpes, University Savoie Mont Blanc; 1130 Rue de la Piscine, 38610 Gières, France*

Corresponding author : pierre-antoine.bonnefont@grenoble-inp.fr

October 14, 2024

Abstract

The mechanism and kinetics of the electrochemical oxidation of glucose on gold surfaces in 0.1 M NaOH solution are investigated by rotating disc electrode and differential electrochemical mass spectrometry coupled to microkinetic modelling. For this purpose, the glucose mass-transport parameters (solution viscosity and density, glucose diffusion coefficient) were determined in the relevant conditions. Koutecký-Levich analysis of rotating disc electrode current-potential curves revealed that the glucose oxidation reaction (GOR) follows a one-electron mechanism at 0.6 V *vs* RHE, while H_2 production could be evidenced by DEMS in this potential range. This suggests that the glucose oxidation selectively produces gluconate at 0.6 V *vs* RHE through an electrochemical oxidative dehydrogenation (EOD) mechanism. A microkinetic model of the current-potential curves was developed, taking into account the hydrogen electrode reactions kinetics, the dissociative adsorption/desorption of glucose, and the glucose electrooxidation on gold surfaces. The dissociative adsorption of glucose was found to be the rate-determining step of the reaction. It is also revealed that the release of anodic H_2 through the Tafel step is triggered by the consumption of the adsorbed reaction intermediates. The gluconate electrooxidation into further products has to be considered for potential above 0.7 V *vs* RHE.

Graphical abstract

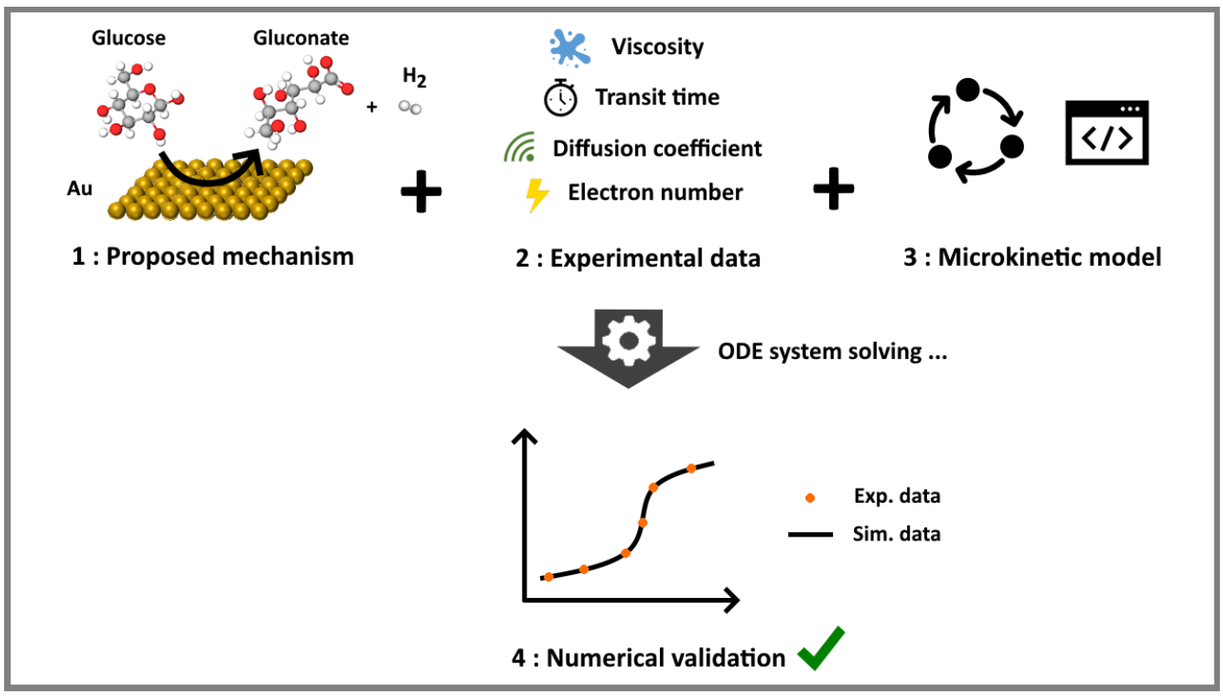

Keywords

Glucose oxidation reaction (GOR), microkinetic modelling, glucose diffusion coefficient, gluconate, electrochemical oxidative dehydrogenation (EOD).

Highlights

- The glucose diffusion coefficient was determined in 0.1 M NaOH.
- The GOR follows an electrooxidative dehydrogenation process on gold at 0.6 V *vs* RHE.
- The rate-determining step of the GOR is glucose dissociative adsorption.
- The H_2 anodic production is triggered by the oxidation of GOR adsorbed intermediates.

1 Introduction

Fine chemistry massively relies on fossil fuels, used as feedstock [1]. In order to respond to current environmental challenges, a change in raw material is necessary. Glucose is a promising carbon source, that can be used as an alternative raw material [2]. It can be extracted by hydrolysis [3] from lignocellulosic biomass [4]

(a renewable resource) such as agricultural waste, urban wood waste or industrial organic waste. Then, as a biomass-derived platform molecule, it can be transformed into many value-added products such as fumaric acid, itaconic acid, malic acid, arabinose and 5-hydroxymethylfurfural (HMF) among many others [5, 6], but also into gluconic acid [7], the latter having a wide range of applications in food, health, textile and cosmetic industries [8].

Due to its possible applications, the glucose oxidation reaction (GOR) has been studied on many catalysts [9] and especially on noble metals such as Ag, Ir and Rh [10], but also Pd [11, 12, 13] and Pt [14, 15, 16]. Among those catalysts, Au demonstrated very promising properties for the selective oxidation of glucose into gluconate [17, 18]. In a recent contribution, it was shown that the glucose oxidation is accompanied by anodic hydrogen production, as evidenced by differential electrochemical mass spectrometry (DEMS) measurements [18]. This process, called electrochemical oxidative dehydrogenation (EOD) [19], involves C-H bond cleavage and H_2 desorption from the recombination of the adsorbed hydrogen H_{ad}, through a Tafel step.

Although the glucose oxidation into gluconate on gold is generally considered as a 2-electron mechanism [20], Koutecký-Levich (KL) analysis of rotating disc electrode current-potential curves recently revealed that only 1 electron is exchanged per glucose molecule for the early stages of the glucose oxidation reaction [21], which is consistent with the electrochemical oxidative dehydrogenation of aldehydes to carboxylates discussed by Ramos *et al.* [19].

Despite numerous studies, the EOD mechanism is still under discussion. In the case of hydroxymethylfurfural electrooxidation, it was suggested that gem-diolate formed through the reaction of aldehyde with OH^- is the active species [22]. Kinetic isotope effect studies have shown that the C-H bond cleavage is involved in the rate determining step [23]. Besides, it was suggested that the formation of anodic H_2 is favored by the displacement of H_{ad} by OH^- adsorption [24], the Tafel step being then faster than the H_{ad} oxidation to form H_2O (Volmer step).

In this contribution, we study the kinetics of the GOR on gold surfaces by employing rotating (ring) disc electrode, differential electrochemical mass spectrometry and microkinetic modelling. First, the evaluation of the number of exchanged

electrons by a KL study relies on the value of the glucose diffusion coefficient. To the best of our knowledge, no accurate data for the glucose diffusion coefficient in alkaline media are currently available: a value of 6.7 10^{-6} cm^2 s^{-1} (at infinite dilution in water at 25°C) is given by the CRC Handbook of Chemistry and Physics [25], while a much higher value (calculated as a mean over experiments measured at various concentrations and at room temperature) is proposed by Hassaninejad-Darzi *et al.* [26]. The actual value of the glucose diffusion coefficient is evaluated using a rotating ring disk electrode (RRDE) under relevant conditions for the study of the glucose oxidation reaction, and an updated Koutecký-Levich analysis is proposed.

Then, a mean field microkinetic model of the glucose oxidation reaction (GOR) on gold is developed to provide insight into the EOD kinetics. The GOR reaction steps used in the microkinetic model are based on the mechanism previously proposed by Medrano-Banda *et al.* [21]. To account for the glucose mass-transport, the model relies on viscosity and diffusion coefficient values, that were determined in the relevant conditions. The kinetic parameters of the hydrogen evolution reaction (HER) on Au electrode are adjusted using the current-potential curves obtained in supporting electrolyte in the absence of glucose. These parameters were used in the model of the glucose oxidation reaction to simulate the anodic H_2 production observed by DEMS. By confronting the experimental data to the microkinetic simulations, we conclude that the glucose dissociative adsorption is the rate-determining step of the GOR on Au surfaces. Analyzing the rates of the steps involved in the GOR reveals that the anodic H_2 production occurs through the Tafel step and is triggered by the consumption of the adsorbed intermediates of the GOR. Finally, the gluconate oxidation has to be taken into account for potential above 0.7 *vs* RHE.

2 Experimental

2.1 Materials

All solutions were prepared using ultrapure water (Milli-Q, resistivity > 18.2 MΩ cm, < 3 ppb TOC) and purged using 5.0 purity argon from Messer. *D*-(+)-glucose ($\geq$ 99.5% purity) was purchased from Sigma Aldrich, and sodium hydroxide solution (50% w/w) from Alfa Aesar. All chemicals were used as received, without

further purification. Au sputtering targets (4N purity) used for the thin film deposition for DEMS experiments were purchased from Neyco.

2.2 Physical parameters determination

The dynamic viscosity (μ, mPa s or cP) of the electrolyte (1, 5 or 10 mM glucose in 0.1 M NaOH) was determined using a viscometer Brookfield Fungilab Alpha, thermostated at 10, 25 and 40°C. A series of volumic mass (ρ, g cm^{-3}) measurements were performed in the same conditions, using a LASER densimeter (Anton Paar DMA 4101). Out of these measurements, the kinematic viscosity (ν, cm^2 s^{-1}) of the electrolyte was determined using the well-known relation $\nu = \mu/\rho$. This physical parameter of the electrolyte allows then accessing the diffusion coefficient, through the use of a rotating ring disk electrode (RRDE).

2.3 Electrochemical measurements

RRDE measurements

The rotating ring disk electrode (RRDE) can be used under certain conditions to determine the diffusion coefficient of an electroactive species. The measurement method, described in details elsewhere [27, 28, 29], relies on the so-called transit time (t_s) measured between the application of a potential perturbation at the disk electrode, and its effect measured at the ring. This transit time can be expressed as:

$$t_s = K \left(\frac{\nu}{D}\right)^{1/3} \omega^{-1} \quad \text{where} \quad K = 43.1 \left(\log\left[\frac{D_{ir}}{D_{od}}\right]\right)^{2/3} \tag{1}$$

Thus, the transit time t_s (s) depends on the previously determined kinematic viscosity of the electrolyte (ν, cm^2 s^{-1}), the diffusion coefficient of the electroactive species (D, cm^2 s^{-1}) and the rotation speed of the electrode (ω, rpm). The geometry of the RRDE is accounted *via* K (s.rpm). Here, the internal diameter of the ring (D_{ir}) and external diameter of the disc (D_{od}) were measured respectively at 4.96 and 4.57 mm, *i.e.* $K = 4.661$. A series of measurements made by a VSP 95 potentiostat at various rotation rate will then allow plotting t_s *vs* ω^{-1}, the slope of the straight line obtained giving access to the diffusion coefficient of the electroactive specie. An example of a series of measures is given in section 4.1.

RDE measurements

Once the glucose diffusion coefficient is known at the relevant concentration and temperature, in the actual electrolyte (NaOH 0.1 M), it is possible to determine the number of exchanged electrons through a Koutecký-Levich study. To that goal, cyclic voltammetry measurements were performed at 10 mV s^{-1} and at rooom temperature, on a rotating disk electrode (RDE) equipped with a 1 µm mirror-polished gold disk of 2 mm diameter, dipped into a 1 mM glucose + 0.1 M NaOH solution. By expressing I_k the kinetically-limited current and I_L the mass-transport limited current, one obtain at a given potential [30]:

$$\frac{1}{I} = \frac{1}{I_k} + \frac{1}{I_L} = \frac{1}{I_k} + \frac{1}{0.62\ z\ F\ A\ D^{2/3}\ \nu^{-1/6}\ C\ \omega^{1/2}} \tag{2}$$

where I is the measured current (mA), z is the number of electrons exchanged, F the Faraday constant (96485 C mol^{-1}), A the geometric surface of the electrode (cm^2), D the diffusion coefficient of the electroactive species (cm^2 s^{-1}), ν the kinematic viscosity of the electrolyte (cm^2 s^{-1}), C the electrolyte concentration in electroactive species (mol L^{-1}) and ω the rotation speed of the electrode (rad s^{-1}). Again, a series of CV acquired at various rotation rate will allow plotting $1/I$ *vs* $\omega^{-1/2}$, the slope of the straight line obtained giving access to the number of exchanged electrons, z.

2.4 DEMS measurements

Differential Electrochemical Mass Spectrometry (DEMS) was used to probe hydrogen production (H_2, $M/z = 2$) during cyclic voltammetry, performed with a VMP2Z potentiostat. The mass spectrometer (QME 220, Pfeiffer Vacuum) is separated from the cell by a porous steel frit, supporting 3 layers of porous hydrophobic PTFE membrane (Cobetter PF-002H, 20 µm thickness, 20 nm pore diameter) to ensure water tightness. The working electrode (WE) was either a RDE, either a 50 nm thick gold film deposited onto the upper PTFE membrane, see section 4.3. Detailed deposition procedure and cell description are given elsewhere [18], and the choice of the relevant WE is discussed in the results section. A 2 cm^2 glassy carbon plate held by a gold wire was used as counter electrode, and a commercial RHE (Gaskatel HydroFlex) was used as reference electrode (RE). The RE was coupled to an auxiliary electrode (a Pt wire) through two capacitors (22

µF each) to act as a filter for high frequency noise [31] generated by the DEMS setup, and especially the turbo-molecular pumps.

3 Microkinetic model development

3.1 Parameters definition

C_i is defined as the interfacial concentration of the species i, and C_i^* its concentration in the bulk. These low values (in the order of magnitude of 10^{-5} mol cm^{-3}) can lead to significant numerical errors during resolution. To avoid so, $C_\mathrm{ref} = 10^{-5}$ mol cm^{-3} and $C^0 = 1$ mol cm^{-3} are defined as normalization concentrations, and the model will use dimensionless (through C^0) and normalized (through C_ref) concentrations: $[i] = \frac{C_\mathrm{i}/C^0}{C_\mathrm{ref}/C^0} = \frac{C_\mathrm{i}}{C_\mathrm{ref}}$ and $[i]^* = \frac{C_\mathrm{i}^*/C^0}{C_\mathrm{ref}/C^0} = \frac{C_\mathrm{i}^*}{C_\mathrm{ref}}$.

Besides, θ_i is defined as the surface coverage in specie i. For the simple species (H, OH, O), a single surface site is considered as covered by their adsorption. For the significantly larger species (gluconate and dissociated glucose), n_s adjacent sites will be considered as occupied. Finally, a non-dissociated glucose molecule requires $n_\mathrm{s} + 1$ available sites to be adsorbed. Glu-H, Glu and Gla will designate respectively non-dissociated glucose, dissociated glucose, and gluconate. From this, one obtains the free sites (s) fraction: $\theta_\mathrm{s} = 1 - \theta_\mathrm{H} - \theta_\mathrm{OH} - \theta_\mathrm{O} - n_\mathrm{s} * \theta_\mathrm{Glu} - n_\mathrm{s} * \theta_\mathrm{Gla}$

In order to simplify the notations, we write $f = \frac{F}{RT}$ as the reduced Faraday constant. It will be used preferentially in all notations for the future and we will note S_t the surface density of atoms (mol cm^{-2}). This value defines the number of sites available on the surface of the electrode, and the calculation of its value (for a perfectly flat surface) is detailed in supporting information, section SI.3.2. The real surface having a roughness R_f, we will take $S_\mathrm{t,\,real} = S_\mathrm{t,\,flat} \times R_\mathrm{f}$ for the model.

3.2 Modelled reactions

From the mechanism proposed in a previous contribution [21], 9 steps were taken into account for this model, as depicted in Fig. 1.

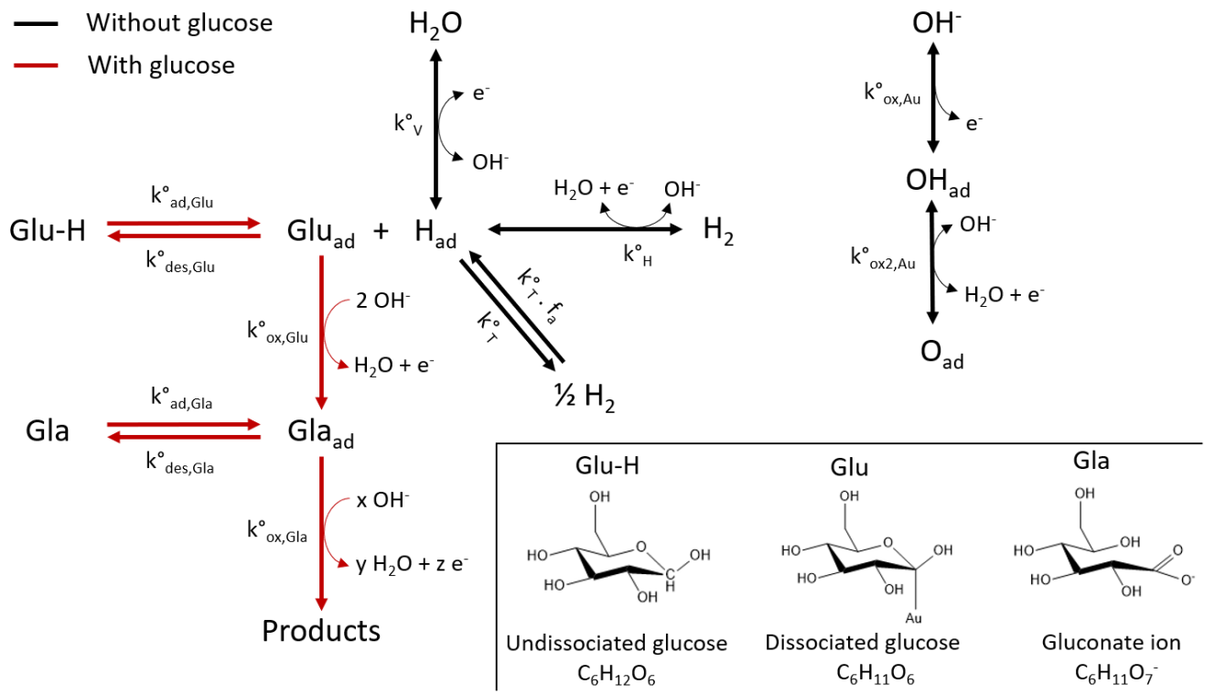

Figure 1. Modelled reactions in absence (supporting electrolyte, black lines) or in presence (red lines) of 10 mM glucose in NaOH 0.1 M.

The HER mechanism comprises the Volmer, Heyrovský and Tafel elementary steps:

$$\text{Volmer:} \quad \mathrm{H_{ad} + OH^-} \underset{1-\alpha_V}{\overset{k_V^\circ \; E_V \; \alpha_V}{\rightleftharpoons}} \mathrm{H_2O + e^- + s} \tag{3}$$

$$\text{Heyrovský:} \quad \mathrm{H_2 + OH^- + s} \underset{1-\alpha_H}{\overset{k_H^\circ \; E_H \; \alpha_H}{\rightleftharpoons}} \mathrm{H_2O + H_{ad} + e^-} \tag{4}$$

$$\text{Tafel:} \quad \mathrm{2\,H_{ad}} \underset{k_T^\circ . f_a}{\overset{k_T^\circ}{\rightleftharpoons}} \mathrm{H_2 + 2\,s} \tag{5}$$

k_V° and k_H° are defined as the kinetic constants of the Volmer and Heyrovský steps, respectively. In the same way, α_V and α_H are defined as the charge-transfer symmetry coefficients of the Volmer and Heyrovský steps, in the direct direction, while E_V and E_H are the standard potentials of these steps. Concerning the Tafel step, we define f_a as the ratio between the kinetic constant in the backward direction and the kinetic constant in the forward direction. By taking k_T° the kinetic constant in the forward direction, we then obtain $k_T^\circ . f_a$ the kinetic constant in the backward direction. Finally, in the absence of information on local pH variations during the reaction, the $[OH^-]$ concentration is kept constant. It will therefore not be involved in the expression of reaction rates, as well as H_2O. Thus, the reaction rates are written:

$$\text{Volmer:} \quad v_{\mathrm{V}} = k_{\mathrm{V}}^{\circ}\Big(\theta_{\mathrm{H}}\ e^{\alpha_{\mathrm{V}} f(E_{\mathrm{dl}}-E_{\mathrm{V}})} - \theta_{\mathrm{s}}\ e^{-(1-\alpha_{\mathrm{V}}) f(E_{\mathrm{dl}}-E_{\mathrm{V}})}\Big) \tag{6}$$

$$\text{Heyrovský:} \quad v_{\mathrm{H}} = k_{\mathrm{H}}^{\circ}\Big(\frac{C_{\mathrm{ref}}}{C^0}\ [\mathrm{H_2}]\ \theta_{\mathrm{s}}\ e^{\alpha_{\mathrm{H}} f(E_{\mathrm{dl}}-E_{\mathrm{H}})} - \theta_{\mathrm{H}}\ e^{-(1-\alpha_{\mathrm{H}}) f(E_{\mathrm{dl}}-E_{\mathrm{H}})}\Big) \tag{7}$$

$$\text{Tafel:} \quad v_{\mathrm{T}} = k_{\mathrm{T}}^{\circ}\ \theta_{\mathrm{H}}^{\ 2} - k_{\mathrm{T}}^{\circ} f_a\ \frac{C_{\mathrm{ref}}}{C^0}\ [\mathrm{H_2}]\ \theta_{\mathrm{s}}^{\ 2} \tag{8}$$

In order to take into account the thermodynamic potential of the couple H_2O/H_2 (equal to 0 V *vs* RHE for a H_2 pressure of 1 bar, the hydrogen concentration in the electrolyte then being $[H_2]_{\mathrm{sat}}$), there is a relationship between E_{V}, E_{H} and f_{a} at thermodynamic equilibrium and in stationary conditions (see supporting information, section SI.3.1). From that, we derive the expression of f_{a} (see Eq. SI.6):

$$f_{\mathrm{a}} = \frac{e^{2fE_{\mathrm{V}}}}{\frac{C_{\mathrm{ref}}}{C^0}\ [\mathrm{H_2}]_{\mathrm{sat}}} \tag{9}$$

together with the expression of the standard potential of the Heyrovský step (see Eq. SI.12):

$$E_{\mathrm{H}} = \frac{\ln\big(\frac{C_{\mathrm{ref}}}{C^0}\ [\mathrm{H_2}]_{\mathrm{sat}}\big)}{f} - E_{\mathrm{V}} \tag{10}$$

These relations therefore make it possible to ensure that $E_{\mathrm{dl}} = 0$ V corresponds to 0 V *vs* RHE. The other parameters (k_{V}°, k_{H}°, k_{T}°, α_{V} and α_{H}) are adjusted to reproduce the experimental behavior measured in the HER potential zone.

At high potential, the formation of surface hydroxides and oxides are considered on Au surface:

$$\text{Hydroxides:} \quad \mathrm{OH^-} + \mathrm{s} \ \underset{\swarrow}{\overset{k_{\mathrm{ox,Au}}^{\circ}\ E_{\mathrm{ox,Au}}}{\rightleftharpoons}}\ \mathrm{OH_{ad}} + \mathrm{e^-} \tag{11}$$

$$\text{Oxides:} \quad \mathrm{OH_{ad}} + \mathrm{OH^-} \ \underset{\swarrow}{\overset{k_{\mathrm{ox_2,Au}}^{\circ}\ E_{\mathrm{ox_2,Au}}}{\rightleftharpoons}}\ \mathrm{O_{ad}} + \mathrm{H_2O} + \mathrm{e^-} \tag{12}$$

As before, we define $k_{\mathrm{ox,Au}}^{\circ}$ and $k_{\mathrm{ox_2,Au}}^{\circ}$ the kinetic constants associated with the formation of hydroxides and oxides, respectively. In the same way, we express $E_{\mathrm{ox,Au}}$ and $E_{\mathrm{ox_2,Au}}$ the associated standard potentials. The reaction rates are then written as:

$$\text{Hydroxides:} \quad v_{\text{ox,Au}} = k^{\circ}_{\text{ox,Au}}\Big(\theta_{\text{s}}\ e^{\alpha f(E_{\text{dl}}-E_{\text{ox,Au}})} - \theta_{\text{OH}}\ e^{-(1-\alpha)f(E_{\text{dl}}-E_{\text{ox,Au}})}\Big) \tag{13}$$

$$\text{Oxides:} \quad v_{\text{ox}_2\text{,Au}} = k^{\circ}_{\text{ox}_2\text{,Au}}\Big(\theta_{\text{OH}}\ e^{\alpha f(E_{\text{dl}}-E_{\text{ox}_2\text{,Au}})} - \theta_{\text{O}}\ e^{-(1-\alpha)f(E_{\text{dl}}-E_{\text{ox}_2\text{,Au}})}\Big) \tag{14}$$

In a first approximation, the charge-transfer symmetry coefficients α are taken equal to 0.5 here, as in the rest of the model. In order to reproduce as faithfully as possible the plateau observed at high potential, a Frumkin interaction parameter constant (g) was introduced into the expression of the oxide formation rate. This constant did not improve the simulations, so we considered a Langmuir adsorption isotherm ($g = 0$) for simplicity.

In the presence of glucose, new reaction steps must obviously be considered. First of all, we will consider the dissociative adsorption/desorption of glucose (Glu), but also the adsorption/desorption of the gluconate ion ($C_6H_{11}O_7^-$, Gla). These reactions are written:

$$\text{Glucose:} \quad \text{Glu}{-}\text{H} + (\text{n}_\text{s} + 1\,) \cdot \text{s} \ \underset{k^{\circ}_{\text{des,Glu}}}{\overset{k^{\circ}_{\text{ad,Glu}}}{\rightleftharpoons}}\ \text{Glu}_\text{ad} + \text{H}_\text{ad} \tag{15}$$

$$\text{Gluconate:} \quad \text{Gla} + \text{n}_\text{s} \cdot \text{s} \ \underset{k^{\circ}_{\text{des,Gla}}}{\overset{k^{\circ}_{\text{ad,Gla}}}{\rightleftharpoons}}\ \text{Gla}_\text{ad} \tag{16}$$

It should be mentioned that the GOR reaction steps considered in the microkinetic model might comprise several elementary processes, especially the dissociative adsorption of glucose on gold. For the sake of simplicity, it is considered as a single step. We note $k^{\circ}_{\text{ad,i}}$ and $k^{\circ}_{\text{des,i}}$ the kinetic constants of adsorption and desorption of the specie i, respectively. The adsorption of a glucose molecule requires $n_s + 1$ free sites: n_s sites are covered by the glucose adsorbate itself, and an additional site is needed to form the adsorbate H_{ad}, by dissociative adsorption. Gluconate produced by oxidation of glucose therefore releases n_s sites when it desorbs. The associated reaction rates are then written as:

$$\text{Glucose:} \quad v_{\text{ad,Glu}} = k^{\circ}_{\text{ad,Glu}}\ \frac{C_{\text{ref}}}{C^0}\ [\text{Glu-H}]\ {\theta_{\text{s}}}^{(n_\text{s}+1)} - k^{\circ}_{\text{des,Glu}}\ \theta_{\text{Glu}}\ \theta_{\text{H}} \tag{17}$$

$$\text{Gluconate:} \quad v_{\text{ad,Gla}} = k^{\circ}_{\text{ad,Gla}}\ \frac{C_{\text{ref}}}{C^0}\ [\text{Gla}]\ {\theta_{\text{s}}}^{n_\text{s}} - k^{\circ}_{\text{des,Gla}}\ \theta_{\text{Gla}} \tag{18}$$

For the sake of consistency, we noted here [Glu-H] the normalized concentration of glucose (not dissociated), at the interface. In the following we will simply write [Glu], the coverage rate of (dissociated) glucose adsorbate being written θ_{Glu} and therefore cannot be confused.

The second category of reactions to consider are adsorbate oxidation reactions. Since no reduction current (excluding HER) is measured in the potential range considered, these reactions are considered irreversible. For glucose, we have two possible oxidation reactions: a direct oxidation (1 step) with two hydroxide ions in solution (which releases an electron) and a two-step oxidation which involves an adsorbate $\mathrm{OH_{ad}}$, the electron being then released during its adsorption. As no effect of considering both paths distinctly was observed on the simulated data, we will only take into account the global reaction, corresponding to the 1 step process:

$$\mathrm{Glu_{ad}} + 2\,\mathrm{OH^-} \xrightarrow{k^\circ_{\mathrm{ox,Glu}}} \mathrm{Gla_{ad}} + \mathrm{H_2O} + \mathrm{e^-} \tag{19}$$

We denote by $k^\circ_{\mathrm{ox,Glu}}$ the kinetic constant of the glucose oxidation into gluconate ion ($\mathrm{C_6H_{11}O_7^-}_{\mathrm{ad}}$, denoted by $\mathrm{Gla_{ad}}$. The electrical charge balance is therefore respected). The reaction rate is then written:

$$v_{\mathrm{ox,Glu}} = k^\circ_{\mathrm{ox,Glu}}\ \theta_{\mathrm{Glu}}\ e^{\alpha f E_{\mathrm{dl}}} \tag{20}$$

This glucose oxidation reaction is insufficient to reproduce the CVs obtained experimentally in the high potential region, see supporting information (Fig. SI.3). It is therefore necessary to consider the oxidation of the gluconate. The detailed mechanism of gluconate oxidation being beyond the scope of this paper, we will only consider a one-step oxidation, which involves only hydroxide ions in solution, although their prior stabilization on the surface is possible. The gluconate oxidation products (which could include glucaric acid [20] and xylonic acid [16]) as well as the number of electrons and $\mathrm{OH^-}$ ions involved are not precisely known, and will not be specified. This reaction is written:

$$\mathrm{Gla_{ad}} + x\ \mathrm{OH^-} \xrightarrow{k^\circ_{\mathrm{ox,Gla}}} \mathrm{Products} + \mathrm{n_s}\cdot\mathrm{s} + y\ \mathrm{H_2O} + z\ \mathrm{e^-} \tag{21}$$

And similarly to the oxidation of glucose, the reaction rate is written:

$$v_{\mathrm{ox,Gla}} = k^{\circ}_{\mathrm{ox,Gla}}\ \theta_{\mathrm{Gla}}\ e^{\alpha f E_{\mathrm{dl}}} \tag{22}$$

The model considered being that of an RDE, the mass-transport in the electrode vicinity takes place in a Nernst diffusion layer. The thickness δ (cm) of this layer depends on the rotation speed ω (rad s^{-1}) of the electrode, but also on the viscosity of the electrolyte ν (cm^2 s^{-1}) and on the diffusion coefficient of the specie i considered D_i (cm^2 s^{-1}), according to the relation [30]:

$$\delta_i = 1.61\ D_i^{1/3}\ \nu^{1/6}\ \omega^{-1/2} \tag{23}$$

We therefore define, for each species, a boundary layer thickness. For gluconate, we will consider a diffusion coefficient value identical to that calculated for glucose. Fick's first law [30] then allows to express the diffusion speed of the species considered here:

$$v_{\mathrm{diff,H_2}} = \frac{D_{\mathrm{H_2}}}{\delta_{\mathrm{H_2}}}\Big([\mathrm{H_2}]^* - [\mathrm{H_2}]\Big) = \frac{D_{\mathrm{H_2}}}{\delta_{\mathrm{H_2}}}\left(\frac{C^*_{\mathrm{H_2}}}{C_{\mathrm{ref}}} - [\mathrm{H_2}]\right) \tag{24}$$

$$v_{\mathrm{diff,Glu}} = \frac{D_{\mathrm{Glu}}}{\delta_{\mathrm{Glu}}}\Big([\mathrm{Glu}]^* - [\mathrm{Glu}]\Big) = \frac{D_{\mathrm{Glu}}}{\delta_{\mathrm{Glu}}}\left(\frac{C^*_{\mathrm{Glu}}}{C_{\mathrm{ref}}} - [\mathrm{Glu}]\right) \tag{25}$$

$$v_{\mathrm{diff,Gla}} = \frac{D_{\mathrm{Gla}}}{\delta_{\mathrm{Gla}}}\Big([\mathrm{Gla}]^* - [\mathrm{Gla}]\Big) = \frac{D_{\mathrm{Gla}}}{\delta_{\mathrm{Gla}}}\left(\frac{C^*_{\mathrm{Gla}}}{C_{\mathrm{ref}}} - [\mathrm{Gla}]\right) \tag{26}$$

3.3 ODE system definition

All the reactions taken into account previously, and in particular the associated reaction rates, make it possible to define the system of ordinary differential equations (ODE), which describes the behavior of the system over time. Variations in the coverage rate of each species result directly from the reaction rates, which lead to the formation (counted positively) or consumption (counted negatively) of the adsorbates considered. We then express:

$$\frac{d\theta_{\mathrm{H}}}{dt} = v_{\mathrm{H}} - v_{\mathrm{V}} - 2\ v_{\mathrm{T}} + v_{\mathrm{ad,Glu}} \tag{27}$$

$$\frac{d\theta_{\mathrm{OH}}}{dt} = v_{\mathrm{ox,Au}} - v_{\mathrm{ox_2,Au}} \tag{28}$$

$$\frac{d\theta_{\mathrm{O}}}{dt} = v_{\mathrm{ox_2,Au}} \tag{29}$$

$$\frac{d\theta_{\mathrm{Glu}}}{dt} = v_{\mathrm{ad,Glu}} - v_{\mathrm{ox,Glu}} \tag{30}$$

$$\frac{d\theta_{\mathrm{Gla}}}{dt} = v_{\mathrm{ox,Glu}} + v_{\mathrm{ad,Gla}} - v_{\mathrm{ox,Gla}} \tag{31}$$

and rely on the work of Koper *et al.* [32], subsequently refined by Berthier *et al.* [33] in order to express the variations in interfacial concentrations (normalized) to hydrogen, glucose and gluconate, as follows:

$$\frac{d[\mathrm{H_2}]}{dt} = \frac{\pi^2}{4\ \delta_{\mathrm{H_2}}} \times \left(\frac{S_{\mathrm{t}}}{C_{\mathrm{ref}}}\ (v_{\mathrm{T}} - v_{\mathrm{H}}) + v_{\mathrm{diff,H_2}} \right) \tag{32}$$

$$\frac{d[\mathrm{Glu}]}{dt} = \frac{\pi^2}{4\ \delta_{\mathrm{Glu}}} \times \left(-\ \frac{S_{\mathrm{t}}}{C_{\mathrm{ref}}}\ v_{\mathrm{ad,Glu}} + v_{\mathrm{diff,Glu}} \right) \tag{33}$$

$$\frac{d[\mathrm{Gla}]}{dt} = \frac{\pi^2}{4\ \delta_{\mathrm{Gla}}} \times \left(-\ \frac{S_{\mathrm{t}}}{C_{\mathrm{ref}}}\ v_{\mathrm{ad,Gla}} + v_{\mathrm{diff,Gla}} \right) \tag{34}$$

Moreover, the variation of the applied potential (U) simply corresponds to the (arithmetic) scan rate v_{s}.

$$\frac{dU}{dt} = v_{\mathrm{s}} \tag{35}$$

Finally, the variation of the double-layer potential (E_{dl}) is deduced from the equivalent electrical diagram of the electrode (Fig. 2), which involves the double-layer capacitance (C_{dl}), the charge-transfer resistance (R_{ct}) and the electrolyte resistance (R_{Ω}):

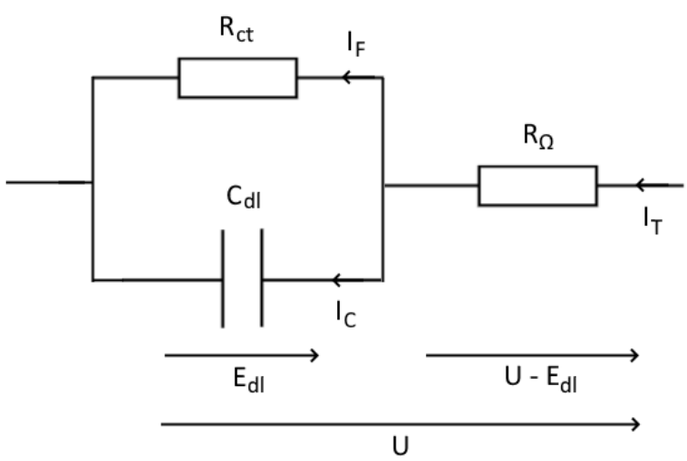

Figure 2. Equivalent electrical diagram of the electrode.

The total current (I_{T}) is expressed according to Ohm's law, but can also be expressed as the sum of the faradic current (I_{F}) and the capacitive current (I_{dl}). We obtain:

$$I_{\mathrm{T}} = I_{\mathrm{F}} + I_{\mathrm{dl}} \Leftrightarrow \frac{U - E_{\mathrm{dl}}}{R_{\Omega}} = I_{\mathrm{F}} + C_{\mathrm{dl}} \frac{dE_{\mathrm{dl}}}{dt} \tag{36}$$

After rearrangement and expressing I_{F} according to the rate of the steps which produce or consume some electrons, we finally obtain:

$$\frac{dE_{\mathrm{dl}}}{dt} = \frac{-F\ S_{\mathrm{t}}\ A}{C_{\mathrm{dl}}} \left(v_{\mathrm{V}} + v_{\mathrm{H}} + v_{\mathrm{ox,Au}} + v_{\mathrm{ox_2,Au}} + v_{\mathrm{ox,Glu}} + z\ v_{\mathrm{ox,Gla}} \right) + \frac{U - E_{\mathrm{dl}}}{C_{\mathrm{dl}}\ R_{\Omega}} \tag{37}$$

The set of eqs. (27) to (35) and (37) forms the ODE system to solve. This system of equations was coded in Scilab (v 2023.1.0), and a brief calculation (depending on the potential limits, the scan rate, and the desired temporal resolution) makes it possible to obtain the time vector corresponding to a scan (positive or negative). Once the initial conditions are fixed, the 'ode' solver implemented in Scilab makes it possible to solve the system of differential equations for each step of the time vector, therefore at each potential of the scan considered. The 'ode' function will be called with the 'stiff' option (which allows sudden variations to be finely resolved, such as when reactivating the surface for example) and with a relative tolerance on the solutions obtained of $1\ 10^{-12}$. In order to optimize calculation times, the initial conditions are set at 1.5 V *vs* RHE, and the first scan calculated is therefore the return scan (negative arithmetic scan rate). At the end of this calculation, the scan rate is inverted (now positive), the values obtained at -0.5 V *vs* RHE (lower limit) are used as the new initial conditions, and a second resolution of the equations system allows to obtain the forward sweep.

After each resolution of a scan, we directly obtain the applied potential, the double layer potential, and the surface coverage for each species. We deduce from that the total current (see Eq. 36) as well as the equivalent current of hydrogen generated (DEMS). The latter is calculated from the hydrogen flow (taken from the diffusion speed) according to Faraday's law and is expressed as:

$$I_{\mathrm{eq,H_2}} = -2\ F\ A\ C_{\mathrm{ref}}\ v_{\mathrm{diff,H_2}} \times \mathrm{H_{cor}} \tag{38}$$

where A is the geometric surface of the electrode. The factor H_{cor} makes it possible to correct the modeled hydrogen current so that it corresponds to the values measured in the supporting electrolyte, according to the calibration constant. The same H_{cor} value is used in the presence of glucose.

The list of the parameters used to solve the ODE system and their values is given in Appendix A.

4 Results and discussion

4.1 Diffusion coefficient determination

The dynamic viscosity and volumetric mass density measurements were performed at 10, 25 and 40°C, with 0.1 M NaOH solution containing 1, 5 or 10 mM glucose. Raw results of these measurements and the calculated kinematic viscosity are given in supporting information, Tab. SI.1, Tab. SI.2 and Tab. SI.3, respectively. As previously described, a series of measurement was performed on a gold-gold RRDE, the ring being polarized at 1 V *vs* RHE during 20 s, and the disk being polarized first at 0 V *vs* RHE (from 0 to 10 s) and then at 1 V *vs* RHE (from 10 to 20 s). Each measure was repeated 3 times to ensure repeatability, and an example of series is given Fig. 3.

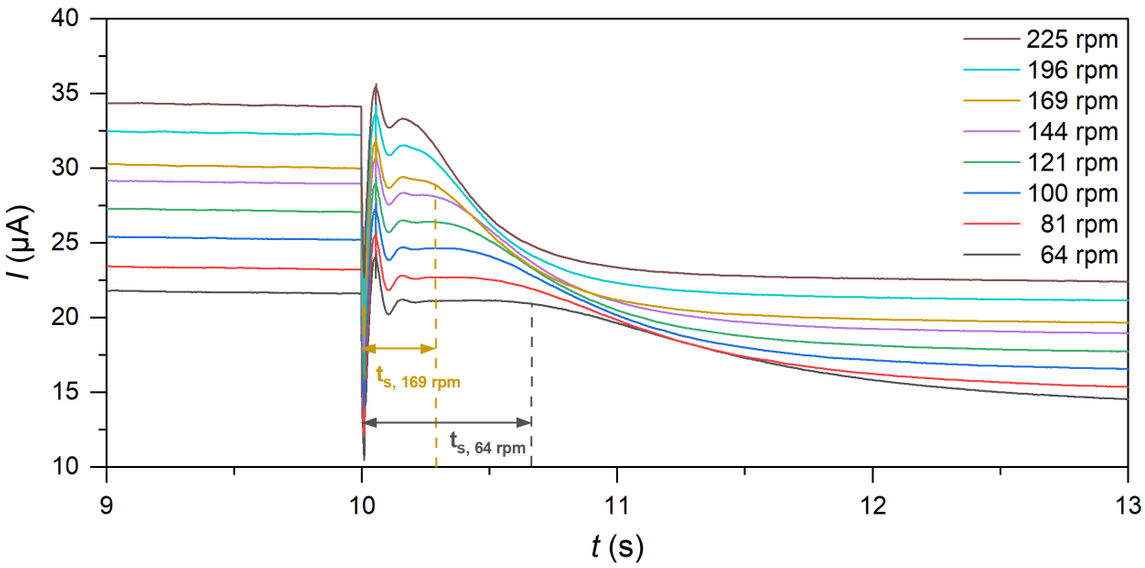

Figure 3. One series of measures performed at the gold ring of a RRDE, dipped into 0.1 M NaOH + 1 mM glucose, at 25°C. The transit times t_s measured at 64 and 169 rpm are given as illustration, and a detailed description of the calculation procedure is given in supporting information, Fig. SI.1.

As expected, the current measured before disk polarisation (at 10 s) increases with the rotation rate, due to an increased mass-transport. After polarization,

the transit time t_s decreases with the rotation rate, also due to a faster mass-transport. Out of these measurements, the transit time was plotted *vs* ω^{-1} for each condition (10, 25 and 40°C, 1, 5 and 10 mM glucose) and showed excellent linearity, the minimum R^2 value obtained from the linear fit being 0.9960. The treated data are given in supporting information, Fig. SI.2. Combining the slope of the linear fit to the previously determined kinematic viscosity allows to calculate the glucose diffusion coefficient, as synthesized in Tab. 1.

Table 1. Glucose diffusion coefficient in 0.1 M NaOH calculated from RRDE measurements.

***D*, 10^{-5} cm^2 s^{-1}**		**Temperature**		
		10°C	25°C	40°C
Conc.	1 mM	0.68	1.68	2.85
	5 mM	1.00	1.43	2.21
	10 mM	1.13	1.27	1.79

These values were compared to the few values available in the literature in Fig. 4.

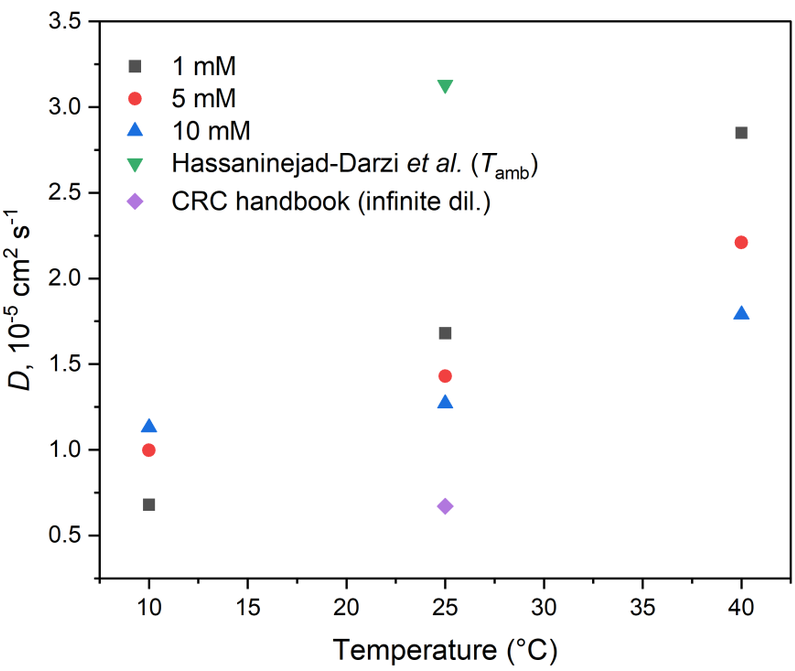

Figure 4. Glucose diffusion coefficient measured by RRDE as function of the temperature, compared to the values available in the literature.

The glucose diffusion coefficient values found by RRDE are comprised between those proposed by the CRC Handbook of Chemistry and Physics [25] and Hassaninejad-Darzi *et al.* [26]. As expected, the apparent diffusion coefficient is higher at higher temperature, the species having a better mobility. This effect is

reduced with increasing glucose concentration, due to an increasing viscosity of the electrolyte, which has an adverse effect on the species mobility. Surprisingly, this trend is inverted at low temperatures (10°C), where the electrolyte containing the highest glucose concentration exhibits the highest apparent diffusion coefficient. This could be tentatively attributed to a temperature-dependant modification of the water structure by glucose [34]. Although they require to be reproduced by other groups to be confirmed, these values are, to the best of our knowledge, the most relevant available data for the determination of the glucose oxidation mechanism.

4.2 Electron number determination

A series of voltammograms was measured at 10 mV s^{-1} on a gold RDE, in presence of 1 mM glucose and at room temperature. Then, as previously described, a Koutecký-Levich (KL) study was performed at potentials ranging from 0.60 to 1.18 V *vs* RHE. The raw voltammograms and the associated KL plots are given in Fig. 5.

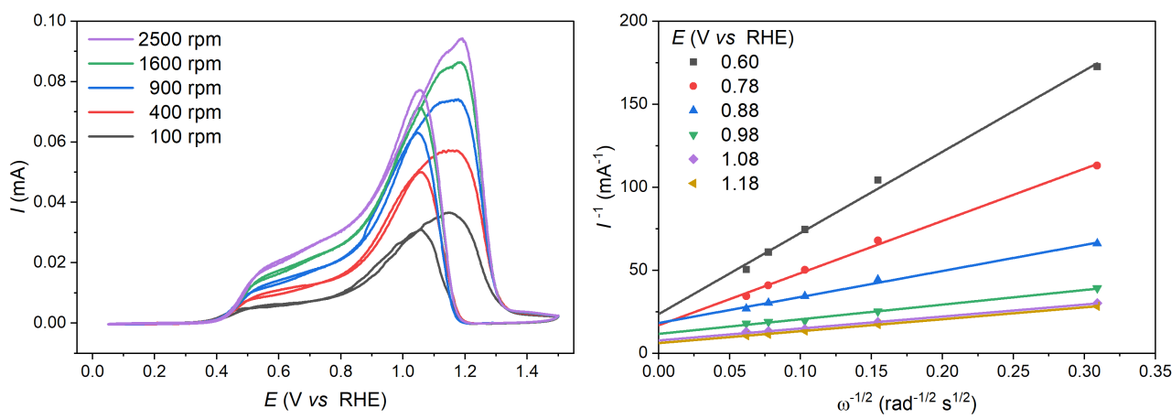

Figure 5. Cyclic voltammograms measured on a gold RDE (2 mm diam.) in 0.1 M NaOH + 1 mM glucose, at 10 mV s^{-1} and at room temperature. Currents are measured during the positive scan for the Koutecký-Levich analysis.

Based on the parameters extracted from the KL plots and on the kinematic viscosity (1.26 10^{-2} cm^2 s^{-1}) and glucose diffusion coefficient (1.68 10^{-5} cm^2 s^{-1}) calculated at 1 mM and 25°C, the number of electrons exchanged during glucose oxidation on gold were calculated as synthesized in Tab. 2.

Table 2. Koutecký-Levich analysis for the GOR on gold.

E (V *vs* RHE)	$1/I_k$ (mA^{-1})	Slope	R^2	Exchanged electrons
0.60	23.6	488	0.9956	0.8
0.78	16.9	314	0.9968	1.3
0.88	18.3	156	0.9945	2.5
0.98	11.8	88.1	0.9922	4.4
1.08	7.79	72.1	0.9961	5.4
1.18	6.21	71.8	0.9996	5.5

These updated calculations of the number of exchanged electrons are in agreement with the proposed mechanism, described in details elsewhere [21] and reproduced in Fig. 1. Roughly one electron per glucose molecule is exchanged at moderate (0.6 V *vs* RHE) potentials, from the oxidation of the adsorbed glucose into gluconate. At this potential, the H_{ad} species formed through the dissociative adsorption of glucose onto the gold surface recombine to produce H_2 through a Tafel step, as confirmed by DEMS. In this case, the GOR equation is: $C_6H_{12}O_6 + 2\,OH^- \rightarrow C_6H_{11}O_7^- + H_2O + \frac{1}{2}\,H_2 + e^-$. At higher potential (0.7 - 0.8 V *vs* RHE), the Volmer step (H_{ad} oxidation into H_2O, with one electron exchanged) becomes faster than the Tafel step, which leads to an overall number of 2 electrons exchanged, according to the equation: $C_6H_{12}O_6 + 3\,OH^- \rightarrow C_6H_{11}O_7^- + 2\,H_2O + 2\,e^-$. With increasing potential, up to 4 additional electrons come from the oxidation of the gluconate species previously formed by glucose oxidation, leading to an overall number of *ca.* 6 electrons exchanged per glucose molecule.

Although the calculated number of electrons agrees with the proposed mechanism, this is insufficient to validate it firmly. To go one step further, the proposed mechanism will be modelled and confronted in a semi-quantitative manner to the experimental data acquired by cyclic voltammetry and DEMS measurements.

4.3 Experimental data acquisition

For simplification reasons, the mass-transport is modelled as for a RDE, with a rotation rate determining the thickness of a diffusion layer at the vicinity of the electrode. This model is perfectly suitable for experiments carried out on a real RDE, with a well-defined rotation rate and mass-transport. However, the experimental data comprised also DEMS data, only measurable in an electrochemical

cell coupled to the mass spectrometer. Then, it has been tried to bring a RDE (used as WE) near the uncoated PTFE membranes of the DEMS, as depicted in Fig. 6.a. In that configuration, the mass-transport was well-defined, but no gaseous species could be detected by the spectrometer. It is likely that the gas dissolution in the solution bulk is faster than its transfer through the PTFE membranes to the DEMS vacuum. A common technique to overcome this limitation is the use of a capillary (diameter typically below 1 mm) as MS inlet, placed very close to the electrode surface (10 µm) as depicted by Briega-Martos *et al.* [35]. In our case, the distance between the RDE tip and the DEMS membrane couldn't be reduced below 1-2 mm due to the experimental configuration, which was therefore discarded. An alternative experimental configuration was preferred (Fig. 6.b), with the use of a gold thin film (deposited onto the PTFE membrane) as WE, ensuring a correct gas collection by the DEMS. A RDE equipped with a PTFE tip was approached to the surface and used as a stirrer to create a "controlled" mass-transport at the vicinity of the WE.

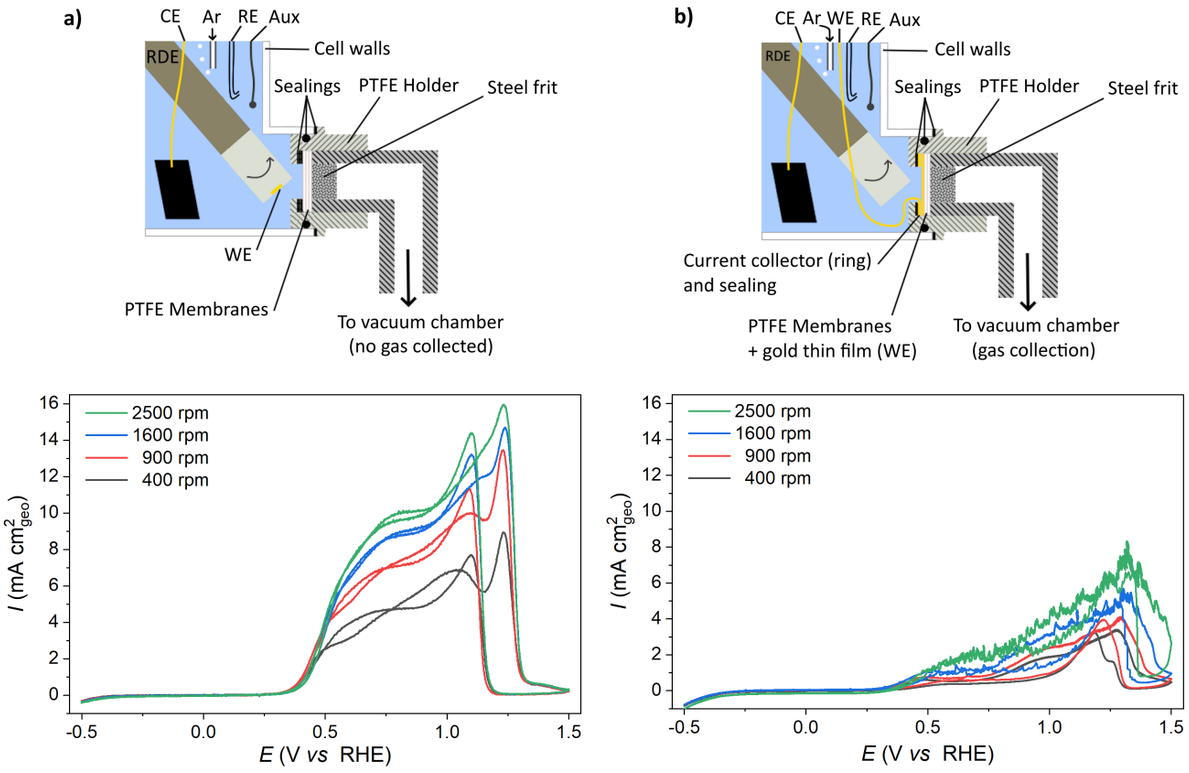

Figure 6. Initial (a) and final (b) configuration of the DEMS + RDE setup, and the associated CV measurements in 0.1 M NaOH + 10 mM glucose. No gaseous species could be detected in configuration a, then the configuration b was preferred.

Although the effect of the rotation rate of the RDE is clearly visible in the chosen configuration (b), the actual mass-transport is significantly lower than on a real RDE rotating at the same speed (a), leading to lower currents. Then, a

correction factor needs to be applied on the actual rotation speed of the RDE used as a stirrer to match the efficient mass-transport produced at the electrode. On a real RDE (configuration a), the mass-transport limited current density ($j_{\mathrm{l,R}}$) is defined by the Levich equation:

$$j_{\mathrm{l,R}} = 0.62\ z\ F\ D^{2/3}\ \nu^{-1/6}\ C\ \omega_{\mathrm{R}}^{1/2} \tag{39}$$

where ω_{R} is the rotation rate of the real RDE. Then, as it will be done for the model, the DEMS porous working electrode (configuration b) is assimilated to a RDE, rotating at $\omega_{\mathrm{D,eq}}$. Thus, the current density measured at the DEMS ($j_{\mathrm{l,D}}$) can be linked through the same equation to the effective mass-transport:

$$j_{\mathrm{l,D}} = 0.62\ z\ F\ D^{2/3}\ \nu^{-1/6}\ C\ \omega_{\mathrm{D,eq}}^{1/2} \tag{40}$$

The experiment being carried at the same potential and in the same electrolyte, any other parameters are kept constant between the configuration a and b, leading to:

$$\frac{j_{\mathrm{l,D}}}{j_{\mathrm{l,R}}} = \left(\frac{\omega_{\mathrm{D,eq}}}{\omega_{\mathrm{R}}}\right)^{1/2} \quad \text{from what} \quad \omega_{\mathrm{D,eq}} = \left(\frac{j_{\mathrm{l,D}}}{j_{\mathrm{l,R}}}\right)^{2} \omega_{\mathrm{R}} \tag{41}$$

Finally, a RDE used as a stirrer (configuration b) generates a mass-transport at the DEMS working electrode equivalent to a real RDE (configuration a) rotating slower, the correction factor being $(j_{\mathrm{l,D}}/j_{\mathrm{l,R}})^2$. This factor was evaluated at 0.6 V *vs* RHE, at every rotation rate. The results are given in Tab. 3.

Table 3. Correction factor of ω at 0.6 V *vs* RHE

ω (rpm)	j_{RDE} (mA $\mathrm{cm}^{-2}_{\mathrm{geo}}$)	j_{DEMS} (mA $\mathrm{cm}^{-2}_{\mathrm{geo}}$)	Factor	$\omega_{\mathrm{D,eq}}$ (rpm)
400	3.62	0.47	59.32	7
900	5.44	0.64	72.25	12
1600	6.61	1.04	40.40	40
2500	7.39	1.62	20.81	120

As expected, the equivalent rotation rate of the fictive RDE is significantly slower that the actual rotation rate of the RDE used as a stirrer, due to less efficient mass-transport. In an ideal case, this factor should be equal to 1 (fully efficient). It seems that at high rotation rate, the factor decreases, from more than 70 (calculated at 900 rpm) to *ca.* 20 at 2500 rpm. The mass-transport efficiency

at the DEMS electrode is then higher at high rotation rate. However, due to the low quality of the CV acquired at high rotation rate, the data obtained at 400 rpm were preferred. At this rotation rate, the correction factor is close to 59, leading to an equivalent rotation rate of 7 rpm. This value will be used in the model to determine the mass-transport conditions, and especially the diffusion layer thickness.

4.4 Simulation of the CV in the absence of glucose

Based on the modelled reactions (Fig. 1) and on the ODE system derived from them (see section 3.3), a first set of simulations were performed in the absence of glucose, to reproduce the experimental data of Au electrodes in 0.1 M NaOH obtained by CV and by DEMS. The experimental results and the optimized simulations are depicted in Fig. 7.

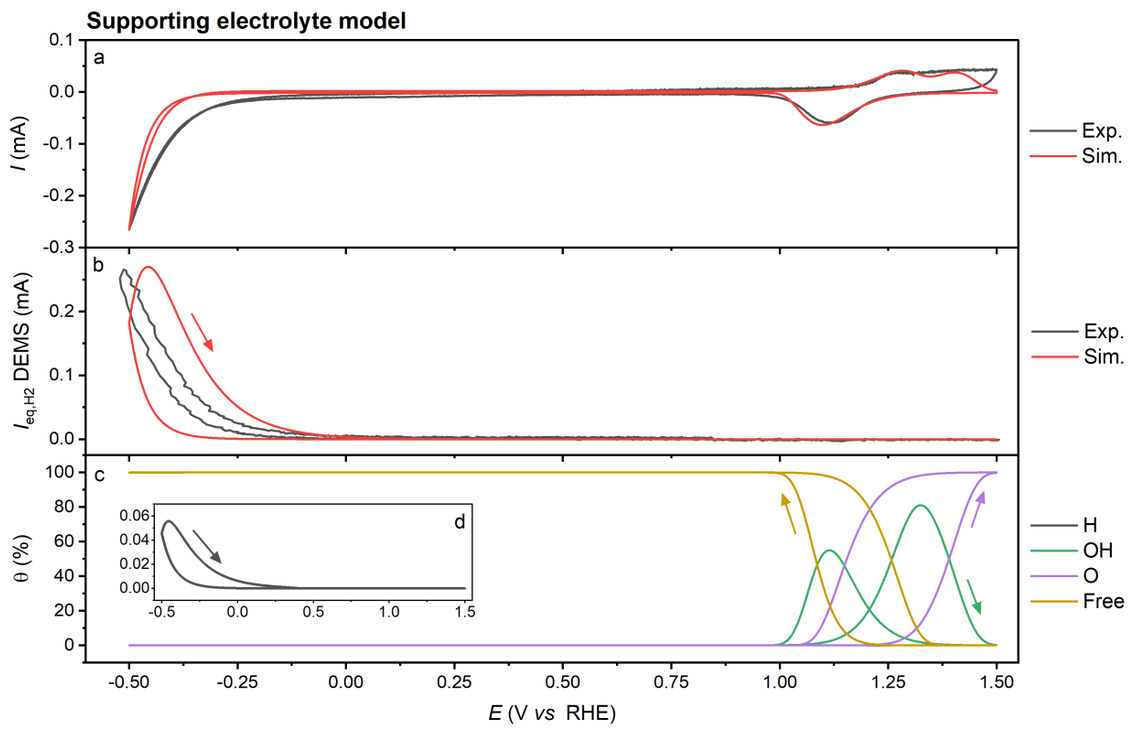

Figure 7. Experimental (black curves) and simulated (red curve) data of a CV (a) and of the associated DEMS signal of H_2 (b) measured at 10 mV s^{-1} in 0.1 M NaOH, at 25°C, under 7 rpm_{eq}. The simulated surface coverage (θ) are given in panel c, and the inset (d) shows a zoom on the adsorbed hydrogen.

Cyclic voltammetry (panel a) reveals the formation of gold hydroxides and then oxides, in the form of a current wave observed at potentials above 1.2 V *vs* RHE. This region is well reproduced by the model, although the shape of the current wave is not completely recovered. During the negative scan, the oxide reduction

peak is faithfully reconstructed by the model. As this peak is integrated (on the experimental data) to evaluate the ECSA and then the surface roughness, its correct description validates the model in the high-potential region. In this potential region, the model predicts (as expected) that the surface is covered with hydroxides (OH, from 1.1 V *vs* RHE) and then oxides (O, from 1.25 V *vs* RHE) during the forward scan, causing the fraction of free sites to decrease to zero. Indeed, at 1.5 V *vs* RHE, the model predicts that the surface is completely covered with gold oxides. During the return sweep, these oxides are reduced to hydroxides and then rapidly reduced again to regenerate free metal sites. This behavior is consistent with the charge measurement of the oxide reduction peak.

At low potential, the Volmer, Tafel and Heyrovský steps taken into account in the model enable us to simulate the experimentally observed HER in the DEMS cell, although it starts *ca.* 100 mV earlier than in the simulations. In the absence of a better indicator, the amount of hydrogen predicted by the model is derived from its diffusion rate in the Nernst layer. However, this assumption leads to an underestimation of the amount of hydrogen produced at -0.5 V *vs* RHE, where the experimental curves have been calibrated. This is consistent with the experimental set-up, as hydrogen is extracted by the DEMS vacuum (additional driving force) and not by diffusion in the Nernst layer. We therefore introduce the corrective factor H_{cor}, which simulates this additional driving force, that could also explain the H_2 detection by DEMS at lower overpotentials than predicted by the model. With this correction factor, the model correctly reconstructs the experimental DEMS signal measured at low potential (panel b), which corresponds to a very low surface coverage rate (of the order of 0.06%) by H_{ad}.

As the model reproduces in a satisfactory way the experimental CV and DEMS data over the potential range studied, its behavior is validated in supporting electrolyte and the kinetic parameters optimized at this stage are fixed for the next simulations.

4.5 Simulation of the CV in the presence of glucose

Following the simulation in supporting electrolyte, a new set of simulated data were produced by taking into account the glucose adsorption/desorption, followed by its oxidation into gluconate. This intermediate version of the model is presented in supporting information (as the partial model, Fig. SI.3) but did not reproduce faithfully the experimental data. Finally, the partial model was completed by accounting for the gluconate oxidation into subsequent products, considering the exchange of 4 electrons per gluconate molecule, in agreement with the KL analysis. The experimental data and the optimized simulations obtained with the complete model are depicted in Fig. 8. The model sensitivity to some of the kinetics parameters is discussed in supporting information, Fig. SI.4.

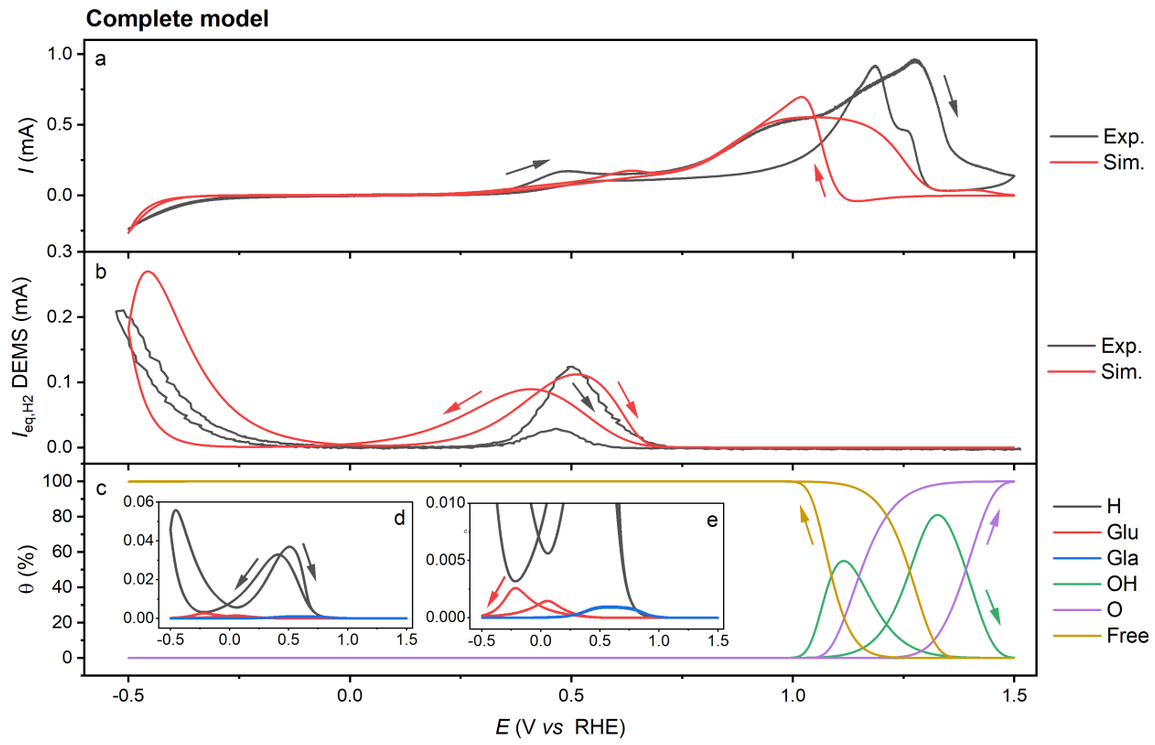

Figure 8. Experimental (black curves) and simulated (red curve) data of a CV (a) and of the associated DEMS signal of H_2 (b) measured at 10 mV s^{-1} in 0.1 M NaOH + 10 mM glucose, at 25°C, under 7 rpm_{eq}. The simulated surface coverage (θ) are given in panel c, and the inset (d and e) shows a zoom on the adsorbed hydrogen, glucose and gluconate.

In the presence of glucose, the experimental curves obtained by CV and DEMS are obviously different from those measured in the absence of glucose, as discussed previously (Fig. 1). At potentials close to 0.5 V *vs* RHE, the model reproduces semi-quantitatively the first oxidation step observed by CV (panel a), as well as the associated hydrogen signal (panel b), which supports the proposed reaction

model. In this range of potentials, the model predicts the transformation of adsorbed glucose into adsorbed gluconate (panel e). Accounting for the gluconate oxidation in the complete model results in a new oxidation wave at potential above 0.7 V *vs* RHE, which better reproduces the experimentally obtained CV (panel a) compared to the partial model (Fig. SI.3). This supports the proposed mechanism, where the glucose oxidation into gluconate (at low potential) precedes the oxidation of the gluconate formed (at high potential), reflecting a loss of selectivity at potentials above 0.7 V *vs* RHE. It is worth noticing that the magnitude of the experimental H_2 escape anodic current peak in the forward scan is well reproduced by the simulation, while the simulated H_2 peak in the backward potential scan is overestimated compared to the experimental one. This might be tentatively attributed to the presence of adsorbed reaction products formed in the high potential region and not considered in the microkinetic model. Further insight into the electrochemical oxidative dehydrogenation (EOD) kinetics can be gained by plotting the reaction rates *vs* the potential, as depicted in Fig. 9

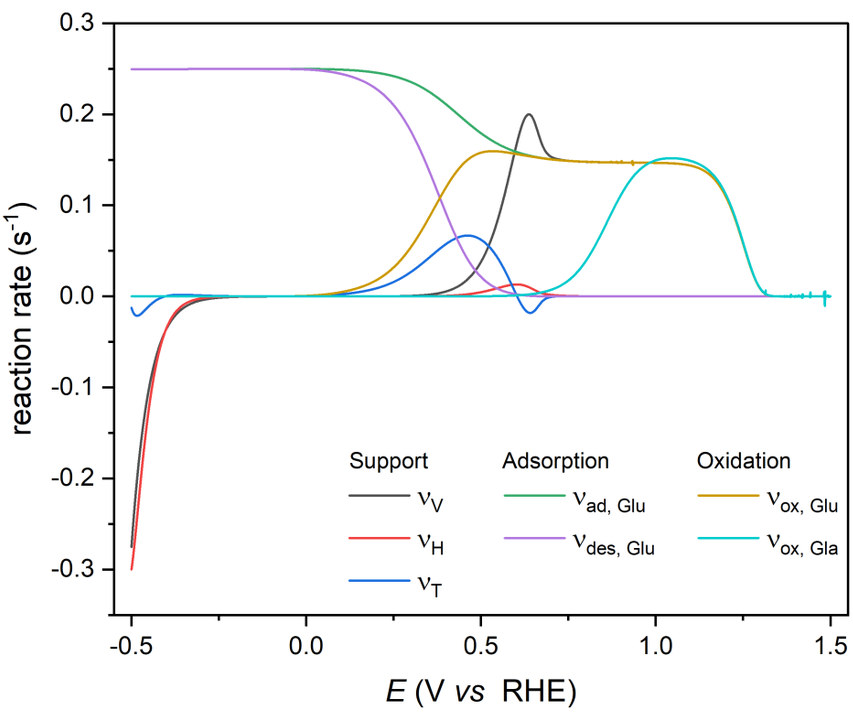

Figure 9. Calculated reaction rates of the Volmer (black), Heyrovský (red) and Tafel (dark blue) steps. The rates of glucose adsorption (green), glucose desorption (purple), glucose oxidation (yellow) and gluconate oxidation (light blue) are also shown. Simulation performed at 10 mV s^{-1} in 0.1 M NaOH + 10 mM glucose, at 25°C, under 7 rpm_{eq}.

Below 0 V *vs* RHE, the hydrogen evolution reaction (HER) on Au electrode mainly follows a Volmer-Heyrovský mechanism, the contribution of the Tafel step

being minor. In that potential region, the rates of glucose adsorption and desorption are balanced. At potentials above 0.2 to 0.3 V *vs* RHE, the product of glucose adsorption starts being oxidized, which provokes the decrease of the glucose adsorbates coverage and their replacement by gluconate adsorbates, as displayed in Fig. 8.e. Consequently, the glucose desorption rate decreases (as less adsorbed glucose molecules are present at the surface) together with the glucose adsorption rate (the surface being partly covered by adsorbed gluconate and H_{ad} species). Due to the oxidation of the glucose adsorbates, the surface coverage in H_{ad} species increases (Fig. 8.d), which increases their recombination rate through a Tafel step as H_2, the maximum being reached close to 0.5 V *vs* RHE. At higher potential (close to 0.7 V *vs* RHE), the rate of the potential activated Volmer step (oxidation of H_{ad}) becomes predominant and leads to the decrease in the H_2 signal detected by DEMS. At such potential, the Volmer step and the glucose oxidation step occurs at the same rate, each step leading to the exchange of one electron, *i.e.* 2 electrons per oxidized glucose molecule. Finally, at potentials higher than 0.7 V *vs* RHE, the gluconate is further oxidized, its oxidation rate being limited by the oxidation rate of glucose.

In addition, it is of interest to discuss the rate-determining step (RDS) of the GOR at 0.6 V *vs* RHE. For a glucose concentration of 10 mM, the maximum glucose dissociative adsorption rate can be estimated by $k^{\circ}_{ad,Glu}\ C_{Glu}/C^0 = 0.25\ s^{-1}$, which is well below the maximum glucose oxidation rate: $k^{\circ}_{ox,Glu}\ e^{\alpha f E_{dl}} = 5.9\ 10^6\ s^{-1}$. Thus, it can be concluded that in the model, the glucose dissociative adsorption is the rate-determining step of the GOR. In reality, the dissociative adsorption might not be an elementary step, and the C-H bond cleavage is proposed to be the rate-determining step [23]. The dissociative adsorption step being the RDS of the model is in line with the sensitivity analysis (See supporting information, Fig. SI.4), in which the adsorption kinetic constant has a major impact on the electrochemical current simulated at 0.6 V *vs* RHE (Fig. SI.4.b), while no significant effect of the oxidation kinetic constant is observed (Fig. SI.4.c). However, the oxidation kinetic constant has a major impact on the simulated H_2 anodic peak, as it favors the production of H_{ad} species.

Although the experimental data were correctly simulated below 1.0 V *vs* RHE, the current model is still not fitting the shape of the current-potential curve above 1.0 V *vs* RHE. In that region, the current decrease observed during the forward scan is due to the formation of gold oxides, occupying the surface. Then, during the backward scan, the electrode reactivates as soon as the oxides are reduced. As the model allows glucose adsorption only into metallic sites, the deactivation/reaction process are shifted to lower potentials compared to the experimental data. Allowing the glucose to adsorb on gold hydroxides might lead to a better reconstruction of the experimental curves in the oxides region (not shown), but would require further experimental evidence. The model also fails to reproduce the irreversibility observed between the forward and backward scans. This irreversibility, which seems to appear at low rotation speeds (see Fig. 6.a), may be due to a poisoning effect by oxidation products, which are better evacuated under high electrolyte flow (real RDE, 400 to 2500 rpm) than in the experimental configuration considered here (fictive RDE, equivalent to 7 rpm).

5 Conclusions

A reaction mechanism of the glucose oxidation into gluconate on gold was proposed in a previous contribution [21]. In order to confront this mechanism with the experimental data, a microkinetic model of the GOR has been developed, based on the measurements of glucose mass-transport parameters and on an updated estimation of the electron number exchanged during the GOR. In particular, the glucose diffusion coefficient calculation was derived from RRDE measurements in 0.1 M NaOH, leading to values ranging from 0.68 10^{-5} cm^2 s^{-1} (at 1 mM and 10°C) to 2.85 10^{-5} cm^2 s^{-1} (at 1 mM and 40°C). The model aims to reproduce numerically the experimental data obtained in a specific DEMS cell, modified to approximate as closely as possible the mass-transport conditions of a RDE (which is the working hypothesis of the model). A correlation between the actual rotating speed and the "effective" rotating speed has thus been used as an input of the model.

The Koutecký-Levich analysis of the RDE data shows that the number of electron per glucose molecule increases from *ca.* 1 at 0.6 V *vs* RHE to 2.5 at 0.88 V *vs* RHE and *ca.* 6 at 1 V *vs* RHE. These findings are consistent with an electrochem-

ical oxidative dehydrogenation (EOD) of the glucose molecule to form gluconate and $\frac{1}{2}\,H_2$ at 0.6 V *vs* RHE, as confirmed by DEMS measurement. When the potential increases above 0.7 V *vs* RHE, the increase of the number of electron is due to the H_2 as well as the gluconate electooxidation. This confirms that the glucose oxidation occurs in several steps, the glucose being selectively oxidized into gluconate at potentials below 0.7 V *vs* RHE, then the gluconate is in its turn oxidized at higher potentials, leading to a loss of selectivity, as measured by HPLC after electrolysis on gold [21].

Further insights on the EOD process could be gained by the microkinetic model. The latter suggests that the anodic hydrogen production is triggered by the consumption of the adsorbed reaction intermediates resulting in an increase of the H_{ad} coverage and the of the rate of the Tafel step. In addition, it is found that the glucose dissociative adsorption is the rate determining step (RDS) of the GOR. This suggests that the C-H bond cleavage might be the RDS of the reaction.

Appendices

A Simulation parameters

Based on the experimental conditions, electrode geometry, experimental setup and expected tolerance for the numerical resolution, a first list of parameters are set as constants, as synthesized in Tab. A.1.

Table A.1. Model constants

Parameter	Value	Source
Global constants		
F	96485 C mol^{-1}	-
R	8.314 J mol^{-1} K^{-1}	-
T	298 K	25°C
α	0.5	Default value
H_{cor}	2.3	-
Electrode parameters		
A	$\sim$ 0.283 cm^2	6 mm diam.
R_f	8	CV data, ECSA / A
C_{dl}	180 10^{-6} F	CV data, I_{dl}
S_t	2.1 $10^{-9} \times R_f$ mol cm^{-2}	Eq. SI.13
Electrolyte parameters		
ν	1.31 10^{-2} cm^2 s^{-1}	Tab. SI.3
R_Ω	20 Ω	ZIR measurements
C_{glu}	1 10^{-5} mol cm^{-3}	10 mM
C_{gla}	0 mol cm^{-3}	0 mM
$C_{H_2,sat}$	7.8 10^{-7} mol cm^{-3}	n_{H_2}/n_{tot} = 1.411 10^{-5} [25]
C_{ref}	1 10^{-5} mol cm^{-3}	10 mM
C^0	1 mol cm^{-3}	-
Solver parameters		
v_s	1 10^{-2} V s^{-1}	10 mV s^{-1}
t_{step}	1 10^{-3} s	1 ms
tol.	1 10^{-12}	-
Mass transport parameters		
ω	0.733 rad s^{-1}	7 rpm, Tab. 3
D_{H_2}	5.11 10^{-5} cm^2 s^{-1}	[25]
D_{glu}	1.27 10^{-5} cm^2 s^{-1}	Tab. 1
D_{gla}	1.27 10^{-5} cm^2 s^{-1}	D_{glu}

These parameters are set initially, as much as possible on the basis of experimental measurements, and are not modified during simulations to obtain the best agreement possible between experimental data and simulation results. They are used to set the framework of the simulation.

A second list of kinetic parameters were chosen and tuned in order to match as mush as possible the experimental curves, first in supporting electrolyte, then

in the presence of glucose. Their optimized values, used for the simulated curves presented in Fig. 7 and 8, are listed in Tab. A.2.

Table A.2. Kinetic parameters of the model

Parameter	Value	Parameter	Value
Volmer		Adsorption (Glucose)	
k°_{V}	5 10^{-4} s^{-1}	$k^\circ_{\mathrm{ad,Glu}}$	2.5 10^{4} s^{-1}
E_{V}	-0.2 V *vs* RHE [36, 37]	$k^\circ_{\mathrm{des,Glu}}$	3 10^{8} s^{-1}
α_{V}	0.45	n_{s}	1
Heyrovský		Oxidation (Glucose)	
k°_{H}	2.7 10^{-1} s^{-1}	$k^\circ_{\mathrm{ox,Glu}}$	50 s^{-1}
E_{H}	$\ln\left(\frac{C_{\mathrm{ref}}}{C^0}\ [\mathrm{H_2}]_{\mathrm{sat}}\right)/f - E_{\mathrm{V}}$		
α_{H}	0.4		
Tafel		Adsorption (Gluconate)	
k°_{T}	1 10^{7} s^{-1}	$k^\circ_{\mathrm{ad,Gla}}$	1 10^{4} s^{-1}
f_{a}	$e^{2fE_{\mathrm{V}}}/(\frac{C_{\mathrm{ref}}}{C^0}\ [\mathrm{H_2}]_{\mathrm{sat}})$	$k^\circ_{\mathrm{des,Gla}}$	2 10^{4} s^{-1}
Gold (Hydr)oxides		Oxidation (Gluconate)	
$k^\circ_{\mathrm{ox,Au}}$	3.5 10^{-2} s^{-1}	$k^\circ_{\mathrm{ox,Gla}}$	1 10^{-3} s^{-1}
$E_{\mathrm{ox,Au}}$	1.18 V *vs* RHE	z	6
$k^\circ_{\mathrm{ox_2,Au}}$	1.5 10^{-2} s^{-1}		
$E_{\mathrm{ox_2,Au}}$	1.27 V *vs* RHE		

Declaration of competing interest

The authors declare that they have no known competing financial interests or personal relationships that could have appeared to influence the work reported in this paper.

Acknowledgements

This study was funded by the French National Research Agency (ANR): grant ANR-20-CE43-0005. The authors acknowledge Emma Mourey, Elia Gaillard, Carla Cochennec and Shuting You for their very helpful contribution to the RRDE measurements. The authors are all expressing their gratitude to Prof. Elena R. Savinova, who has always been an immense source of inspiration in their work and for stimulating discussions that helped the elaboration of this contribution.

CRediT author statement

Théo Faverge: Investigation, Software, Writing - Original Draft, Visualization. **Antoine Bonnefont:** Conceptualization, Software, Writing - Review and Editing. **Marian Chatenet:** Conceptualization, Supervision, Writing - Review and Editing. **Christophe Coutanceau:** Conceptualization, Supervision, Writing - Review and Editing.

References

[1] P. G. Levi, J. M. Cullen, Mapping global flows of chemicals: from fossil fuel feedstocks to chemical products, Environmental Science and Technology 52 (2018) 1725–1734. doi:10.1021/acs.est.7b04573.

[2] T. Werpy, G. Petersen, Top Value Added Chemicals from Biomass: Volume I – Results of Screening for Potential Candidates from Sugars and Synthesis Gas, Tech. rep., US Department of Energy (2004). doi:10.2172/15008859.

[3] B. Yu, G. Fan, S. Zhao, Y. Lu, Q. He, Q. Cheng, J. Yan, B. Chai, G. Song, Simultaneous isolation of cellulose and lignin from wheat straw and catalytic conversion to valuable chemical products, Applied Biological Chemistry 64 (2021) 1–13. doi:10.1186/S13765-020-00579-X.

[4] R. Vinoth Kumar, G. Pugazhenthi, K. Pakshirajan, Petroleum Versus Biorefinery-Based Platform Chemicals, Elsevier Inc., 2016. doi:10.1016/B978-0-12-802980-0.00003-1.

[5] H. Chen, K. Wan, F. Zheng, Z. Zhang, H. Zhang, Y. Zhang, D. Long, Recent Advances in Photocatalytic Transformation of Carbohydrates Into Valuable Platform Chemicals, Frontiers in Chemical Engineering 3 (2021) 615309. doi:10.3389/fceng.2021.615309.

[6] A. T. Adeleye, H. Louis, O. U. Akakuru, I. Joseph, O. C. Enudi, D. P. Michael, A Review on the conversion of levulinic acid and its esters to various useful chemicals, AIMS Energy 7 (2019) 165–185. doi:10.3934/ENERGY.2019.2.165.

[7] L. Z. de Cárdenas, B. Z. de Cárdenas, Production of Organic Acids Via Fermentation of Sugars Generated from Lignocellulosic Biomass, in: Lignocellulosic Biorefining Technologies, John Wiley & Sons, Ltd, 2020, pp. 203–246. doi:10.1002/9781119568858.CH10.

[8] A. M. Cañete-Rodríguez, I. M. Santos-Dueñas, J. E. Jiménez-Hornero, A. Ehrenreich, W. Liebl, I. García-García, Gluconic acid: Properties, production methods and applications—An excellent opportunity for agro-industrial by-products and waste bio-valorization, Process Biochemistry 51 (2016) 1891–1903. doi:10.1016/J.PROCBIO.2016.08.028.

[9] Z. I. Lai, L. Q. Lee, H. Li, Electroreforming of Biomass for Value-Added Products, Micromachines 12 (2021) 1405. doi:10.3390/MI12111405.

[10] Y. B. Vassilyev, O. A. Khazova, N. N. Nikolaeva, Kinetics and mechanism of glucose electrooxidation on different electrode-catalysts: Part II. Effect of the nature of the electrode and the electrooxidation mechanism, Journal of Electroanalytical Chemistry and Interfacial Electrochemistry 196 (1985) 127–144. doi:10.1016/0022-0728(85)85085-3.

[11] C. C. Hu, T. C. Wen, Voltammetric investigation of palladium oxides-II. Their formation / reduction behaviour during glucose oxidation in NaOH, Electrochimica Acta 39 (1994) 2763–2771. doi:10.1016/0013-4686(94)00291-6.

[12] I. Becerik, F. Kadirgan, The electrocatalytic properties of palladium electrodes for the oxidation of d-glucose in alkaline medium, Electrochimica Acta 37 (1992) 2651–2657. doi:10.1016/0013-4686(92)87065-8.

[13] T. Haynes, V. Dubois, S. Hermans, Particle size effect in glucose oxidation with Pd/CB catalysts, Applied Catalysis A: General 542 (2017) 47–54. doi:10.1016/J.APCATA.2017.05.008.

[14] F. Largeaud, K. B. Kokoh, B. Beden, C. Lamy, On the electrochemical reactivity of anomers: electrocatalytic oxidation of α- and β-d-glucose on platinum electrodes in acid and basic media, Journal of Electroanalytical Chemistry 397 (1995) 261–269. doi:10.1016/0022-0728(95)04139-8.

[15] M. F. de Mele, H. A. Videla, A. J. Arvía, The electrooxidation of glucose on platinum electrodes in buffered media, Journal of Electroanalytical Chemistry and Interfacial Electrochemistry 155 (1983) 239–249. doi:10.1016/S0022-0728(83)80479-3.

[16] G. A.B. Mello, W. Cheuquepán, J. M. Feliu, Investigation of reactivity of Pt basal planes towards glucose electro-oxidation in neutral solution (pH 7): structure-sensitivity dependence and mechanistic study, Journal of Electroanalytical Chemistry 878 (2020) 114549. doi:10.1016/J.JELECHEM.2020.114549.

[17] N. Neha, T. Rafaïdeen, T. Faverge, F. Maillard, M. Chatenet, C. Coutanceau, Revisited Mechanisms for Glucose Electrooxidation at Platinum and Gold Nanoparticles, Electrocatalysis 14 (2023) 121–130. doi:10.1007/s12678-022-00774-y.

[18] T. Faverge, B. Gilles, A. Bonnefont, F. Maillard, C. Coutanceau, M. Chatenet, In Situ Investigation of d-Glucose Oxidation into Value-Added Products on Au, Pt, and Pd under Alkaline Conditions: A Comparative Study, ACS Catalysis 13 (2023) 2657–2669. doi:10.1021/ACSCATAL.2C05871.

[19] N. C. Ramos, A. Holewinski, Recent advances in anodic hydrogen production: Electrochemical oxidative dehydrogenation of aldehydes to carboxylates, Current Opinion in Electrochemistry 45 (2024) 101484. doi:10.1016/J.COELEC.2024.101484.

[20] N. Schlegel, G. K. Wiberg, M. Arenz, On the electrooxidation of glucose on gold: Towards an electrochemical glucaric acid production as value-added chemical, Electrochimica Acta 410 (2022) 140023. doi:10.1016/J.ELECTACTA.2022.140023.

[21] A. Medrano-Banda, E. Ginoux, T. Faverge, A. Oshchepkov, A. Bonnefont, M. Chatenet, C. Coutanceau, G. Kéranguéven, P. Cognet, E. Savinova, Electrochemical oxidation of glucose in alkaline environment—A comparative study of Ni and Au electrodes, Electrochimica Acta 487 (2024) 144159. doi:10.1016/J.ELECTACTA.2024.144159.

[22] G. Fu, X. Kang, Y. Zhang, Y. Guo, Z. Li, J. Liu, L. Wang, J. Zhang, X. Z. Fu, J. L. Luo, Capturing critical gem-diol intermediates and hydride transfer for anodic hydrogen production from 5-hydroxymethylfurfural, Nature Communications 2023 14:1 14 (2023) 1–11. doi:10.1038/s41467-023-43704-2.

[23] H. Liu, N. Agrawal, A. Ganguly, Y. Chen, J. Lee, J. Yu, W. Huang, M. Mba Wright, M. J. Janik, W. Li, Ultra-low voltage bipolar hydrogen production from biomass-derived aldehydes and water in membraneless electrolyzers, Energy & Environmental Science 15 (2022) 4175–4189. doi:10.1039/D2EE01427K.

[24] S. B. Scott, A. K. Engstfeld, Z. Jusys, D. Hochfilzer, N. Knøsgaard, D. B. Trimarco, P. C. Vesborg, R. J. Behm, I. Chorkendorff, Anodic molecular hydrogen formation on Ru and Cu electrodes, Catalysis Science & Technology 10 (2020) 6870–6878. doi:10.1039/D0CY01213K.

[25] D. R. Lide, CRC Handbook of Chemistry and Physics, 85th Edition, New York NY : CRC Press, 2004.

[26] S. Karim Hassaninejad-Darzi, F. Yousefi, Electrocatalytic oxidation of glucose on the modified carbon paste electrode with sodalite nanozeolite for fuel cell., Iranian Journal of Hydrogen & Fuel Cell 1 (2015) 47–58. doi:10.22104/IJHFC.2015.177.

[27] S. Bruckenstein, G. A. Feldman, Radial transport times at rotating ring-disk electrodes. Limitations on the detection of electrode intermediates undergoing homogeneous chemical reaction, Journal of Electroanalytical Chemistry 9 (1965) 395–399. doi:10.1016/0022-0728(65)85037-9.

[28] F. Gan, D. T. Chin, Determination of diffusivity and solubility of oxygen in phosphoric acid using a transit time on a rotating ring-disc electrode, Journal of Applied Electrochemistry 23 (1993) 452–455. doi:10.1007/BF00707621.

[29] M. Chatenet, M. B. Molina-Concha, N. El-Kissi, G. Parrour, J. P. Diard, Direct rotating ring-disk measurement of the sodium borohydride diffusion coefficient in sodium hydroxide solutions, Electrochimica Acta 54 (2009) 4426–4435. doi:10.1016/j.electacta.2009.03.019.

[30] A. J. Bard, L. R. Faulkner, Electrochemical Methods: Fundamentals and Applications, 2nd Edition, Wiley, 2001.

[31] C. C. Herrmann, G. G. Perrault, A. A. Pilla, Dual reference electrode for electrochemical pulse studies, Analytical Chemistry 40 (7) (1968) 1173–1174. doi:10.1021/ac60263a011.

[32] M. T. Koper, J. H. Sluyters, Electrochemical oscillators: their description through a mathematical model, Journal of Electroanalytical Chemistry 303 (1991) 73–94. doi:10.1016/0022-0728(91)85117-8.

[33] F. Berthier, J. P. Diard, C. Montella, Hopf bifurcation and sign of the transfer resistance, Electrochimica Acta 44 (1999) 2397–2404. doi:10.1016/S0013-4686(98)00370-3.

[34] M. Hossain, N. Chowdhury, A. Atahar, M. A. B. H. Susan, Water structure modification by D-(+)-glucose at different concentrations and temperatures-effect of mutarotation, RSC Advances 13 (2023) 19195–19206. doi:10.1039/D3RA03081D.

[35] V. Briega-Martos, J. Solla-Gullón, M. T. Koper, E. Herrero, J. M. Feliu, Electrocatalytic enhancement of formic acid oxidation reaction by acetonitrile on well-defined platinum surfaces, Electrochimica Acta 295 (2019) 835–845. doi:10.1016/J.ELECTACTA.2018.11.016.

[36] E. Skúlason, V. Tripkovic, M. E. Björketun, S. Gudmundsdóttir, G. Karlberg, J. Rossmeisl, T. Bligaard, H. Jónsson, J. K. Nørskov, Modeling the electrochemical hydrogen oxidation and evolution reactions on the basis of density functional theory calculations, Journal of Physical Chemistry C 114 (2010) 18182–18197. doi:10.1021/JP1048887.

[37] E. Santos, P. Hindelang, P. Quaino, E. N. Schulz, G. Soldano, W. Schmickler, Hydrogen Electrocatalysis on Single Crystals and on Nanostructured Electrodes, ChemPhysChem 12 (2011) 2274–2279. doi:10.1002/CPHC.201100309.